the Duffing system converges to the desired periodic orbit $\bar{x}$ in the sense that

$$\lim_{t_1 \le t \to \infty} |x - \bar{x}| = 0 \quad \textit{and} \quad \lim_{t_1 \le t \to \infty} |\dot{x} - \dot{\bar{x}}| = 0 .$$

A nonlinear controller can be designed relatively easily. For example, if one picks

$$h(t;\, x, \bar{x}) = K(x - \bar{x}) + 3\bar{x}^2(x - \bar{x}) + 3\bar{x}(x - \bar{x})^2 ,$$

then, using this particular nonlinear control law, the system reduces to

$$\begin{cases} \dot{X} = Y - p_1 X \\ \dot{Y} = -(K + p_2)X - X^3 , \end{cases} \tag{38}$$

and one can easily verify that the Lyapunov function

$$U(X, Y) = \frac{K + p_2}{2} X^2 + \frac{1}{4} X^4 + \frac{1}{2} Y^2 \tag{39}$$

satisfies $\dot{U} \le 0$, where equality holds if and only if $X \equiv 0$ and $Y \equiv 0$. This means that the controlled Duffing equation, Eq. (38) is asymptotically stable, so that $X \to 0$ and $Y \to 0$ as $t \to \infty$, or the goal

$$|x - \bar{x}| \to 0 \quad \text{and} \quad |\dot{x} - \dot{\bar{x}}| \to 0 \qquad (t \to \infty)$$

is achieved.

It has been observed that, in general, a linear feedback controller is much harder to design for the same purpose. Nevertheless, a successful design of linear feedback controllers for the Duffing system has been developed by the present authors [Dong & Chen 1992b], where the target orbit can even be multiperiodic ones. The conventional feedback controller used has the form

$$\begin{bmatrix} u \\ v \end{bmatrix} = - \begin{bmatrix} K_{11} & K_{12} \\ K_{21} & K_{22} \end{bmatrix} \begin{bmatrix} x - \bar{x} \\ y - \bar{y} \end{bmatrix} , \tag{40}$$

which yields the following controlled Duffing equations:

$$\begin{cases} \dot{x} = -K_{11} x + (1 - K_{12}) y + (K_{11}\bar{x} + K_{12}\bar{y}) , \\ \dot{y} = -(K_{21} + p_2)x - x^3 - (K_{22} + p_1)y + (K_{21}\bar{x} + K_{22}\bar{y}) + q\cos(\omega t) . \end{cases} \tag{41}$$

Before determining a suitable controller described by Eq. (40), in the sense of determining the feedback gain matrix $K = [K_{ij}]$, $i, j = 1, 2$, it is clear that one should first guarantee the controlled system itself be stable. Otherwise, instability (or perhaps new chaotic phenomena) may be introduced into the original system. Now, consider the Jacobian of the controlled Duffing equation and observe that a sufficient condition for the stability is that all the roots of its characteristic equation are located on the open left-half plane, which leads to the following conditions:

$$\begin{cases} p_1 + K_{11} + K_{22} > 0 , \\ K_{11}(p_1 + K_{22}) + (1 - K_{12})(K_{21} + p_2 + 3\bar{x}^2) > 0 . \end{cases} \tag{42}$$

Since this system of two inequalities has four unknowns, it usually has non-unique solutions. For simplicity, consider the case where $K_{11} = K_{22} = 0$. Since $p_1 > 0$, the first condition is satisfied and the second becomes

$$(1 - K_{12})(K_{21} + p_2 + 3\bar{x}^2) > 0 .$$

Letting, furthermore, $K_{12} = 0$ gives the simple condition

$$K_{21} > -p_2 - 3\bar{x}^2 , \tag{43}$$

and reduces the controlled Duffing equation to

$$\begin{cases} \dot{x} = y , \\ \dot{y} = -p_2 x - x^3 - p_1 y + q\cos(\omega t) - K_{21}(x - \bar{x}) . \end{cases} \tag{44}$$

Proposition 3. [*Dong & Chen, 1992b*] *A sufficient condition for a stable linear feedback control of the Duffing system in the form of Eq. (35) is given in (43), namely:*

$$K_{21} > -p_2 - 3\bar{x}^2 .$$

To this end, a few remarks are in order.

First, the choice of $K_{11} = K_{12} = K_{22} = 0$ makes sense if one examines the Jacobian J in which he will find that $\bar{y}$ is not explicitly involved. This implies that it is not necessary to control the y-component directly (to track the $\bar{y}$). It will be seen that $y \to \bar{y}$ $(t \to \infty)$ while controlling only the x-component such that $x \to \bar{x}$ $(t \to \infty)$, due to the implicit relations between x and y.

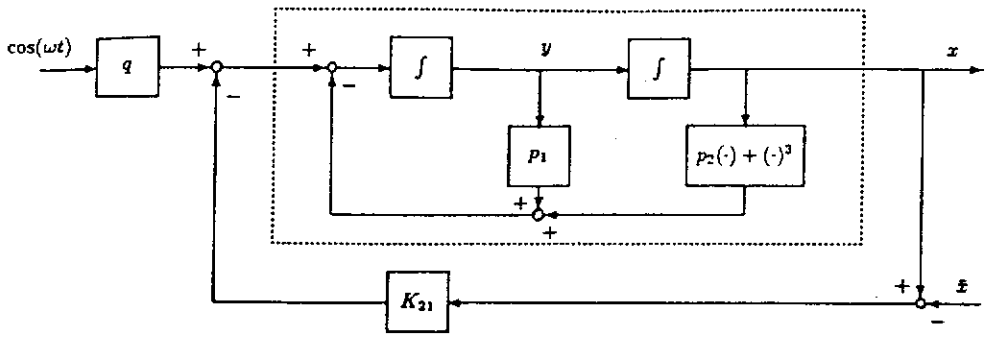

Fig. 21. Implementation of the controlled Duffing system. (*Figure from Dong & Chen [1992b], courtesy of IEEE;* © *1992 IEEE.*)

Second, with the choice of $K_{11} = K_{12} = K_{22} = 0$, the corresponding controlled linearized Duffing equation

$$\begin{bmatrix} \dot{x} \\ \dot{y} \end{bmatrix} = \begin{bmatrix} 0 & 1 \\ -p_2 - 3\bar{x}^2 & -p_1 \end{bmatrix} \begin{bmatrix} x \\ y \end{bmatrix} + \begin{bmatrix} \bar{y} \\ p_1\bar{y} + (p_2 + 3\bar{x}^2)\bar{x} \end{bmatrix} + \begin{bmatrix} 0 \\ 1 \end{bmatrix} v$$

is completely controllable, so that the controlled Duffing equation Eq. (41) is locally controllable, by a conventional feedback of the canonical form (40), namely

$$\begin{bmatrix} 0 \\ 1 \end{bmatrix} v = - \begin{bmatrix} 0 \\ 1 \end{bmatrix} K_{21}[x(t) - \bar{x}(t)] .$$

Simulation results have convinced one that such a simple choice of $K_{11} = K_{12} = K_{22} = 0$ can achieve the control purpose very efficiently. Different choices for the K_{ij}, $i, j = 1, 2$, are of course possible to yield similar results, which in fact may provide more capabilities for other purposes.

Third, using linear feedback controls, one can only guarantee $|x - \dot{x}| \to 0$ but not $|\dot{x} - \dot{\bar{x}}| \to 0$ as $t \to \infty$ (compared with the result given in Theorem 1 above).

Finally, it can be observed that for a (very) large value of K_{21}, called a "high gain," the controlled Duffing Eq. (44) becomes approximately

$$\begin{cases} \dot{x} = y , \\ 0 \approx -K_{21}(x - \bar{x}) , \end{cases} \tag{45}$$

which has a particular solution $(x, y) = (\bar{x}, \dot{\bar{x}})$. This suggests that for (very) large values of the control gain K_{21}, the feedback controller designed above should have (much) better control effect in achieving the goal: $x(t) \to \bar{x}(t)$ $(t \to \infty)$. For small values of K_{21}, however, the oscillatory term $q \cos(\omega t)$ existing originally in the second equation of Eq. (41) may dominate the feedback control input, so that the controlled trajectory appears to be oscillating in some way. This observation has been verified to be true by computer simulations. Hence, in the simulation results to be shown below, a relatively large value for the feedback control gain K_{21} was used. Using different, yet large, values of K_{21} have shown similar results in the simulations. The controlled Duffing equation can be implemented as shown in Fig. 21.

The following are the simulation results of controlling a chaotic trajectory of the Duffing system to its period-1 and period-2 orbits using the feedback-controlled system [Eq. (44)] implemented as in Fig. 21. The control to multiperiodic orbits turns out to be graphically messy and hence will not be further discussed here.

(I) Controlling the chaotic trajectory to a period-1 orbit.

Recall from Fig. 20 that the Duffing equation has multi-periodic orbits. With the parameters $p_1 = 0.4$, $p_2 = -1.1$, $q = 0.21$, and $\omega = 1.8$, the solution trajectory of the equation is chaotic, and with the parameters $p_1 = 0.4$, $p_2 = -1.1$, $q = 0.62$, and $\omega = 1.8$, the equation has a period-1 solution. The goal here is to control the chaotic trajectory of the system to the period-1 orbit.

Figures 22(a) and 22(b) show how the control affects the trajectory of the Duffing system, with $p_1 = 0.4$, $p_2 = -1.1$, $q = 2.1$, and $\omega = 1.8$. Simulations show that the originally chaotic orbits can actually be changed to become nonchaotic and be eventually driven to the target trajectory. In these simulations, the control gain is chosen to be relatively large ($K_{21} = 50.0$), as explained above, in

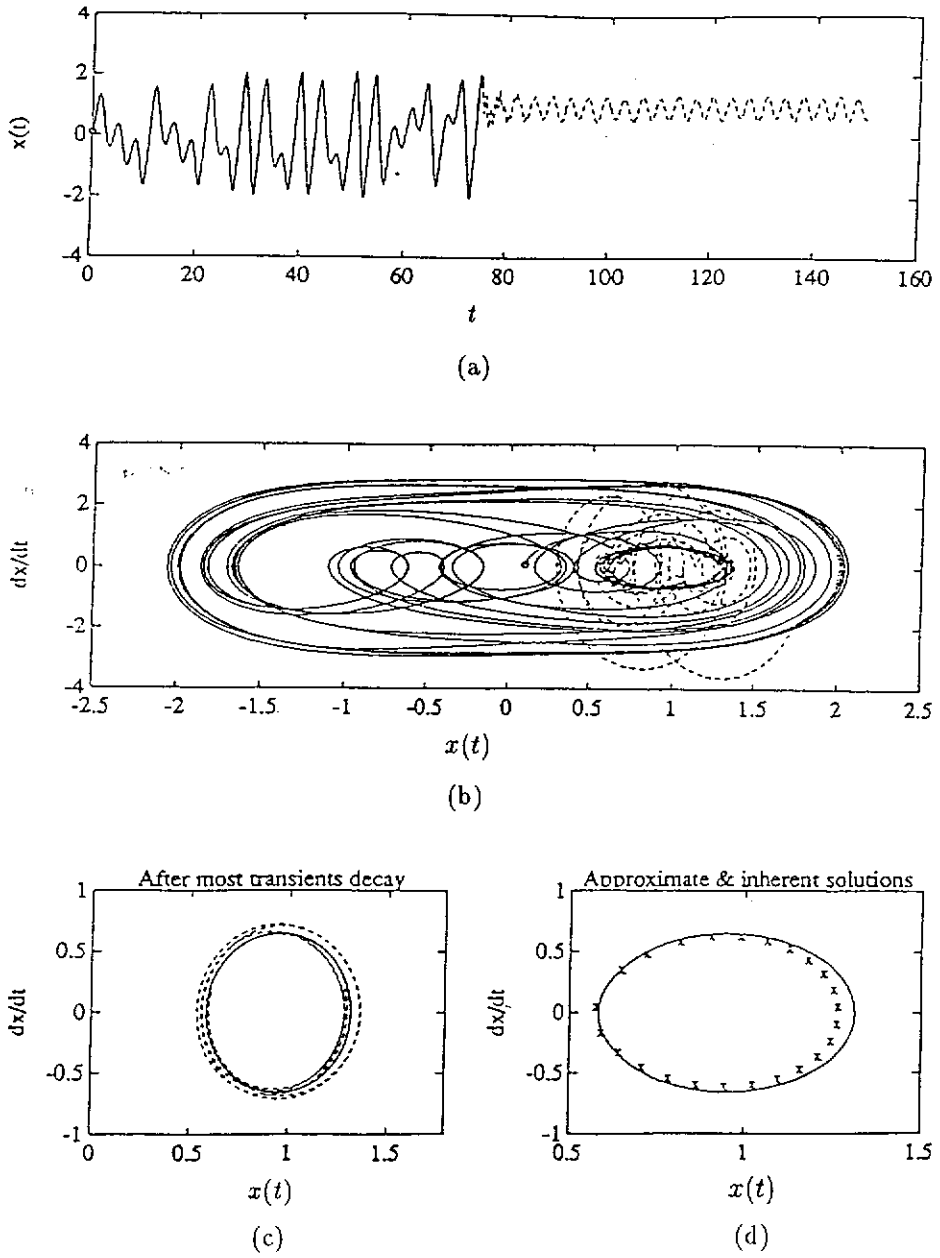

Fig. 22. Controlling Duffing system to a period-1 orbit. (*Figure from Dong & Chen [1992b], courtesy of IEEE; ©1992 IEEE.*)

order to dominate the oscillating term $q\cos(\omega t)$ in the original equation and to obtain better control effect. To show more clearly what happens after applying the control, the region of the target trajectory is enlarged and displayed in Fig. 22(c). The trajectory is plotted after most transients have decayed.

(II) Controlling the chaotic trajectory to a period-2 orbit.

The feedback controller designed above can also drive the chaotic trajectory of the Duffing equation to its period-2 orbit. Recall that with the parameters $p_1 = 0.4$, $p_2 = -1.1$, $q = 2.1$, and $\omega = 1.8$, the solution trajectory of the equation is chaotic, and with the parameters $p_1 = 0.4$, $p_2 = -1.1$, $q = 1.498$, and $\omega = 1.8$, the equation has a period-2 solution. For this control purpose, a high gain $K_{21} = 50.0$ is used. The simulation results are shown in Fig. 23.

4.3. *Controlling Chua's circuit*

Chua's circuit is a simple, yet interesting, electronic system which displays very rich and typical bifurcation and chaotic phenomena such as double scroll, dual double scroll, and double hook [Matsumoto,

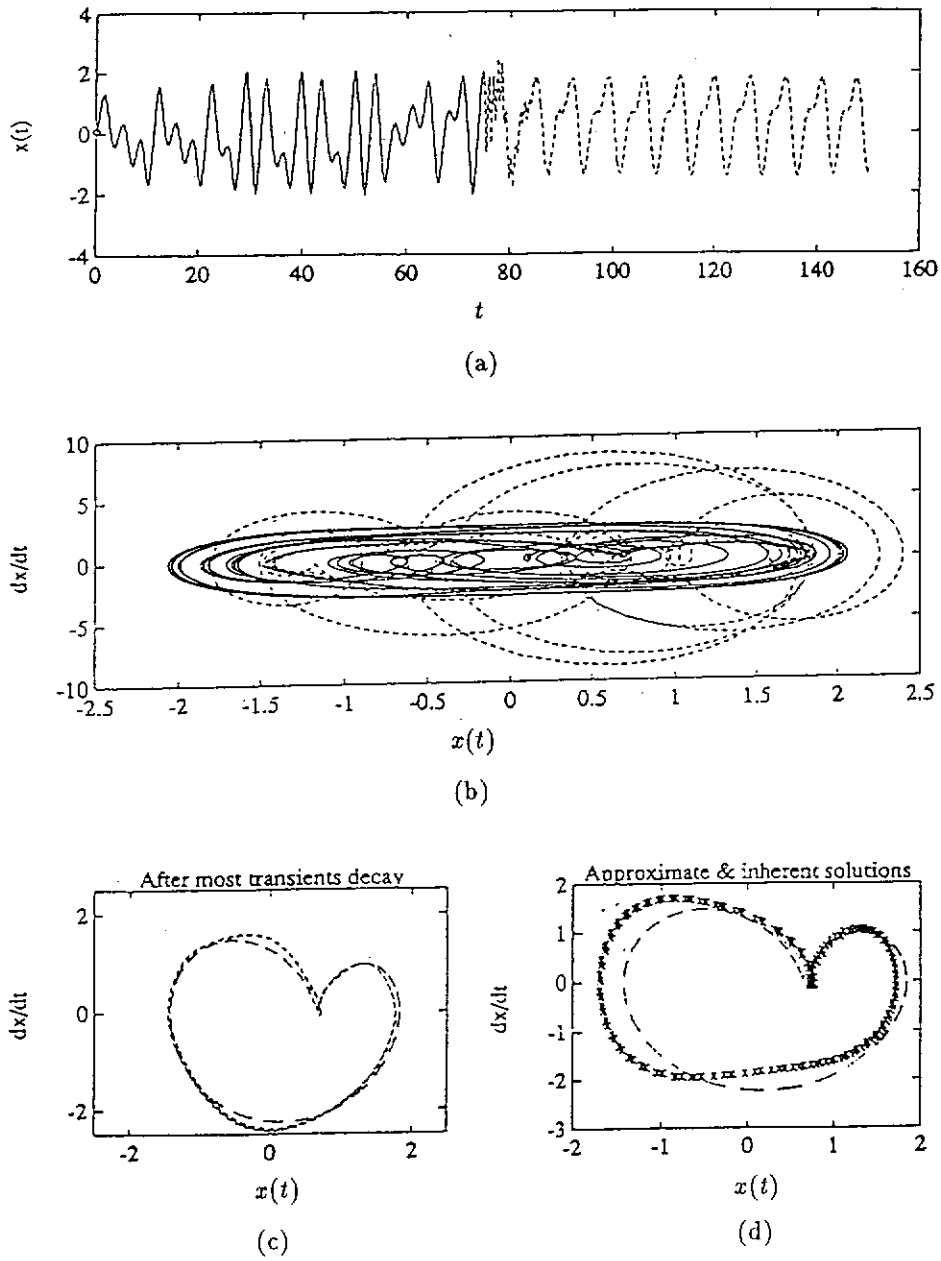

Fig. 23. Controlling Duffing system to a period-2 orbit. (*Figure from Dong & Chen [1992b], courtesy of IEEE; © 1992 IEEE.*)

1984; Matsumoto *et al.*, 1985; Chua *et al.*, 1986; Wu, 1987; Chua, 1992; Kennedy 1992]. The circuit consists of only one inductor (L), two capacitors (C_1, C_2), one linear resistor (G) and one piecewise-linear resistor (g), with the dynamics described by

$$\begin{cases} C_1\dot{v}_{C_1} = G(v_{C_2} - v_{C_1}) - g(v_{C_1}), \\ C_2\dot{v}_{C_2} = G(v_{C_1} - v_{C_2}) + i_L, \\ L\dot{i}_L = -v_{C_2}, \end{cases} \tag{46}$$

where v_{C_1} and v_{C_2} are the voltages across C_1 and C_2 respectively, i_L the current through the inductor L, and the v-i characteristic of the nonlinear resistor is

$$g(v_{C_1}) = g(v_{C_1}; m_0, m_1)$$
$$= m_0 v_{C_1} + \frac{1}{2}(m_1 - m_0)(|v_{C_1}+1| - |v_{C_1}-1|)$$

with $m_0 < 0$ and $m_1 < 0$ being some appropriately chosen constants [Matsumoto *et al.*, 1985].

Reformulate the circuit equation in the following form:

$$\begin{cases} \dot{x} = p[-x + y - f(x)], \\ \dot{y} = x - y + z, \\ \dot{z} = -qy, \end{cases} \tag{47}$$

where $p = (C_2/C_1) > 0$ and $q = (C_2/LG^2) > 0$, and corresponding to the $g(v_{C_1})$ given in the above, $f(x)$ is represented by

$$f(x) = g(x; m_0', m_1') = m_0'x + \frac{1}{2}(m_1' - m_0')(|x+1| - |x-1|),$$

where $m_0' = m_0/G < 0$ and $m_1' = m_1/G < 0$.

Since its first introduction, Chua's circuit and Chua's circuit family have been under considerable investigation as to its dynamical, analytical, experimental or implemental aspects. The nonlinear resistor has now been integrated as an IC chip. Recently, the problem of controlling chaos in Chua's circuit has attracted much attention. We briefly discuss in the following some of the control methods developed for Chua's circuit, and it should be interesting to see how this same problem is studied from different angles by various researchers.

4.3.1. *Linear state feedback control*

The following controllability result, using only linear feedback, has been established by the present authors [Chen & Dong, 1993a]:

Theorem 2. *Let $(\bar{x}, \bar{y}, \bar{z})$ be the unstable limit cycle of Chua's circuit described by Eq. (47) above. Then, the chaotic trajectory (x, y, z) of the circuit can be driven to reach the limit cycle by a simple canonical linear feedback control of the form*

$$\begin{bmatrix} u_1 \\ u_2 \\ u_3 \end{bmatrix} = -K \begin{bmatrix} x-\bar{x} \\ y-\bar{y} \\ z-\bar{z} \end{bmatrix} = - \begin{bmatrix} K_{11} & 0 & 0 \\ 0 & K_{22} & 0 \\ 0 & 0 & K_{33} \end{bmatrix} \begin{bmatrix} x-\bar{x} \\ y-\bar{y} \\ z-\bar{z} \end{bmatrix} \tag{48}$$

with

$$K_{11} \geq -pm_1', \quad K_{22} \geq 0, \quad \text{and} \quad K_{33} \geq 0,$$

where the control can be applied to the trajectory at any time.

The following result was obtained later [Chen & Dong, 1993b]:

Theorem 3. *Let $(\bar{x}, \bar{y}, \bar{z})$ be the unstable limit cycle of Chua's circuit described by Eq. (47). Then, the chaotic trajectory (x, y, z) of the circuit can be driven to reach the limit cycle by a linear feedback control of the form*

$$\begin{bmatrix} u_1 \\ u_2 \\ u_3 \end{bmatrix} = -K \begin{bmatrix} x-\bar{x} \\ y-\bar{y} \\ z-\bar{z} \end{bmatrix} = - \begin{bmatrix} 0 & 0 & 0 \\ 0 & K_{22} & 0 \\ 0 & 0 & 0 \end{bmatrix} \begin{bmatrix} x-\bar{x} \\ y-\bar{y} \\ z-\bar{z} \end{bmatrix}, \tag{49}$$

provided that

$$0 < \frac{1}{m_0'+1} \leq K_{22} \leq -\frac{1}{m_1'+1}.$$

These two theorems only provide sufficient conditions, where, for example, the condition on K_{22} is not always necessary to be so restrictive. The control input of the form equation (49) is among the simplest linear feedback controllers that one can use in Chua's circuit. This simple implementation translates into adding a linear resistor and an appropriate periodic signal generator to the original circuit as shown in Fig. 24.

It is illuminating to examine the performance of the linear feedback controller designed based on

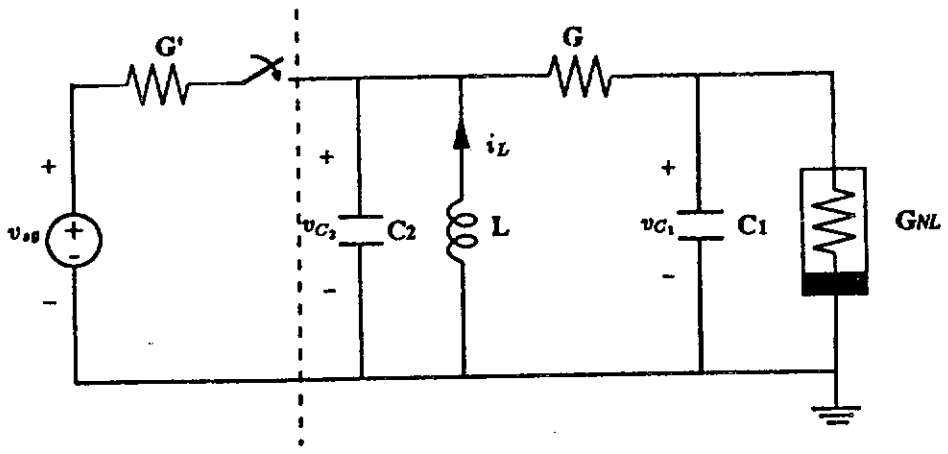

Fig. 24. Implementation of the controlled Chua's circuit. (*Figure from Chen & Dong [1993a].*)

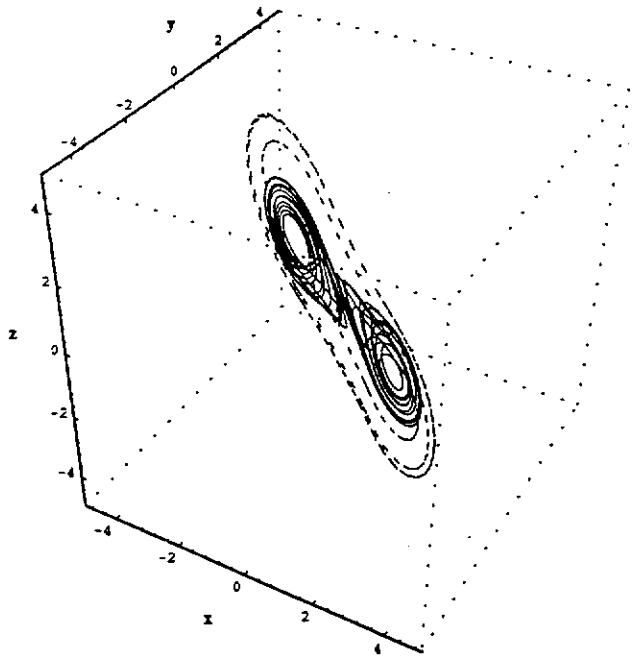

Fig. 25. A solution trajectory of the controlled Chua's circuit. (*Figure from Chen & Dong [1993a].*)

the above theorems and the control process shown in Fig. 25. Under the influence of control, the trajectory is "dragged" out of the double scroll strange attractor and is then directed to gradually approach and eventually reach the intended target, an inherent saddle-type limit cycle of Chua's circuit.

4.3.2. *Targeting unstable steady states and coupling of systems*

Essentially following the parametric variation paradigm, Kapitaniak [1993] made the transformation $p \to p + p^*(t)$ for Chua's circuit, where $p^*(t)$ is regarded as a control function. Let $\mathbf{x} = [x\ y\ z]^\top$. To direct a given chaotic trajectory to one of the stationary points or equilibria ($\mathbf{x}_{sk} = [m\ 0\ -m]^\top$, $[0\ 0\ 0]^\top$, $[-m\ 0\ m]^\top$ where $m = (m_0' - m_1')/(m_0' + 1)$) of Chua's circuit in a finite time T, he considered solving the minimization problem of the regularized cost functional

$$J_\varepsilon(p^*) = \frac{1}{2} \| \mathbf{x}(T, p^*) - \mathbf{x}_{sk} \|_{\mathbf{R}}^2 + \frac{\varepsilon}{2} \| p^* \|_{\mathbf{P}}^2 , \quad (50)$$

where $k = 1, 2, 3$, ε is a small constant, $\| \cdot \|_{\mathbf{R}}$ denotes a norm in $\mathbf{R}^3$ and $\| \cdot \|_{\mathbf{P}}$ a norm in a class $\mathbf{P}$. With the control input assumed to be a quasiperiodic function of the form

$$p^*(t) = \sum_{i=0}^{N} C_i \sin\left(i \frac{\pi T}{t}\right) , \quad (51)$$

where C_i's are constants, he was able to show that a trajectory on the chaotic attractor of Chua's circuit can be steered to the vicinity of a desired stationary state in finite time.

From another perspective, Kapitaniak, Kocarev and Chua demonstrated a method of controlling chaos by coupling a simple, low-dimensional, usually linear, asymptotically stable, autonomous system (controller) to the chaotic system [Kapitaniak *et al.*, 1993]. That is, coupling a chaotic system $\dot{\mathbf{x}} = F(\mathbf{x}, \mu)$ with controller $\dot{\mathbf{y}} = G(\mathbf{y}, \nu)$ (μ is a system parameter) to form the augmented system

$$\begin{cases} \dot{\mathbf{x}} = F(\mathbf{x}, \mu) + M_{\mathbf{y}}\mathbf{y} , \\ \dot{\mathbf{y}} = G(\mathbf{y}, \nu) + M_{\mathbf{x}}\mathbf{x} , \end{cases}$$

where $M_{\mathbf{x}}$ and $M_{\mathbf{y}}$ are some constant matrices and μ and ν are controller parameters. In their experiment, by coupling the Chua's circuit to a second-order linear circuit they modified the circuit into (Fig. 26)

$$\begin{cases} C_1 \dot{v}_{C_1} = G(v_{C_2} - v_{C_1}) - g(v_{C_1}) , \\ C_2 \dot{v}_{C_2} = G(v_{C_1} - v_{C_2}) + i_L + G_x(v_C^{(1)} - v_{C_2}) , \\ L \dot{i}_L = -v_{C_2} , \\ L^{(1)} \dot{i}_L^{(1)} = -v_C^{(1)} , \\ C^{(1)} \dot{v}_C^{(1)} = -G^{(1)} v_C^{(1)} + i_L^{(1)} + G_x(v_{C_2} - v_C^{(1)}) , \end{cases} \quad (52)$$

with notation as defined in the figure. From this augmented system, new stable periodic orbits can be obtained in the neighborhood of the original attractor. In other words, rather than stabilizing the original attractor, the method stabilizes a desired periodic orbit close to that attractor.

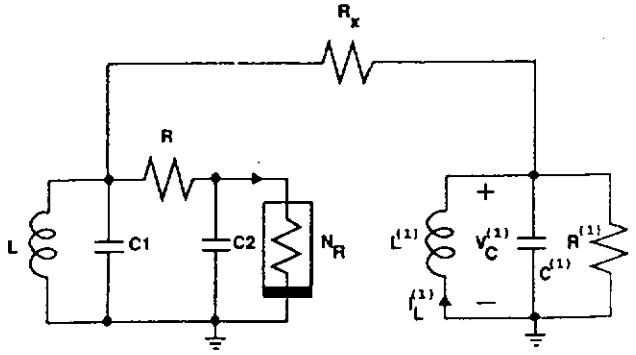

Fig. 26. Chua's circuit coupled with a two-dimensional linear circuit. (*Figure from Kapitaniak, Kocarev & Chua [1993].*)

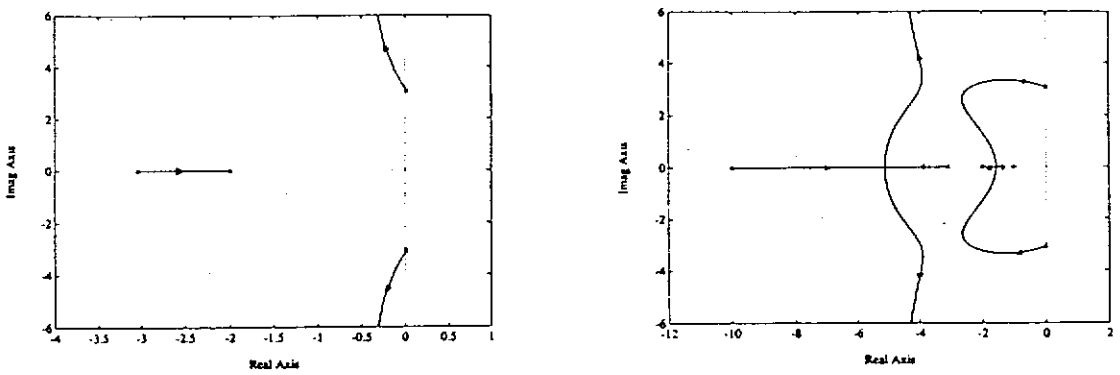

(a) (b)

Fig. 27. (a) Root locus for the y_l-output case; (b) Root locus for the y_l-output case with a lead compensator. (*Figure from Hartley & Mossayebi [1993].*)

4.3.3. *Classical regulators and state space techniques*

Using standard control theory methods, Hartley & Mossayebi [1992, 1993] demonstrated the control of Lorenz and Chua's circuit systems.

In particular, they considered controlling a polynomial variant of the Chua's circuit where the piecewise linear nonlinearity is replaced with a cubic nonlinearity. When a voltage source is added in series with the inductor L, the dynamics of the controlled system is described by

$$\begin{cases} \dot{x} = p[y - n(x)] = p\left[y + \frac{1}{7}(x - 2x^3)\right], \\ \dot{y} = x - y + z, \\ \dot{z} = -qy + u = -\frac{100}{7}y + u, \end{cases} \tag{53}$$

where p and q are system parameters and u represents the control signal. Its equilibrium points are found to be $\mathbf{x}_{sk} = (\sqrt{0.5}, 0, -\sqrt{0.5})$, $(0,0,0)$, and $(-\sqrt{0.5}, 0, \sqrt{0.5})$. The linearized system near the two nonzero equilibria is

$$\begin{bmatrix} \dot{x}_l \\ \dot{y}_l \\ \dot{z}_l \end{bmatrix} = \begin{bmatrix} -\frac{2}{7}p & p & 0 \\ 1 & -1 & 1 \\ 0 & -\frac{100}{7} & 0 \end{bmatrix} \begin{bmatrix} x_l \\ y_l \\ z_l \end{bmatrix} + \begin{bmatrix} 0 \\ 0 \\ 1 \end{bmatrix} u_l, \tag{54}$$

where x_l, y_l, and z_l are the small perturbations from equilibria. When y_l is assumed to be the system output, the small perturbation transfer function is found to be

$$H_y(s) = \frac{Y_l(s)}{U(s)} = \frac{s+2}{s^3 + 3s^2 + \frac{65}{7}s + \frac{200}{7}}, \tag{55}$$

while the transfer functions for x_l or z_l as the outputs can be found similarly. The corresponding root locus can be plotted [Fig. 27(a)] where it can be observed that the stability margin is small. In order to improve the closed-loop performance, a lead compensator $G_{lc}(s) = K(s+1)/(s+10)$ may be used, which results in more robustness in sensitivity due to a larger phase gain [Fig. 27(b)]. When the y-variable is used for feedback, the transfer function is most easily compensated and Fig. 28 shows that the output y approaches the steady state as soon as the control signal $u(t)$ is activated at $t = 40$.

Hartley and Mossayebi also demonstrated how to design a controller for tracking the variable x of the system based on the input-output and state-space techniques. Using state space design approach, the system considered is

$$\begin{cases} \dot{x} = p\left(y + \frac{x - 2x^3}{7}\right), \\ \dot{y} = x - y + z, \\ \dot{z} = -\frac{100}{7}y + u, \\ \dot{w} = r - u, \end{cases} \tag{56}$$

where r is the reference input. To determine the optimal state feedback gain K for the controller $u = -K\mathbf{x} = -[k_x\ k_y\ k_z\ k_w][x\ y\ z\ w]^\top$, a performance index $J = \int_0^\infty (\mathbf{x}^\top Q\mathbf{x} + u^\top Ru)dt$ is used. $K = [1.61\ 0.92\ 1.68\ -1.0]$ can be calculated for $Q = I$, $R = 1$ and the steady state $x_{\text{steady}} = \sqrt{0.5}$. Figure 29 demonstrates the successful tracking.

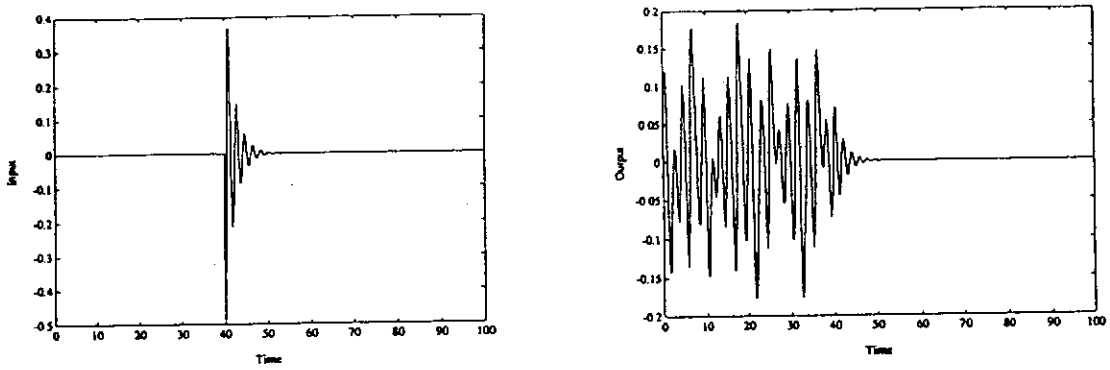

(a) (b)

Fig. 28. (a) Control input $u(t)$; (b) Output $y(t)$. (For the case of lead compensation, $K = 20$, $p = 10$.) (*Figure from Hartley & Mossayebi [1993]*.)

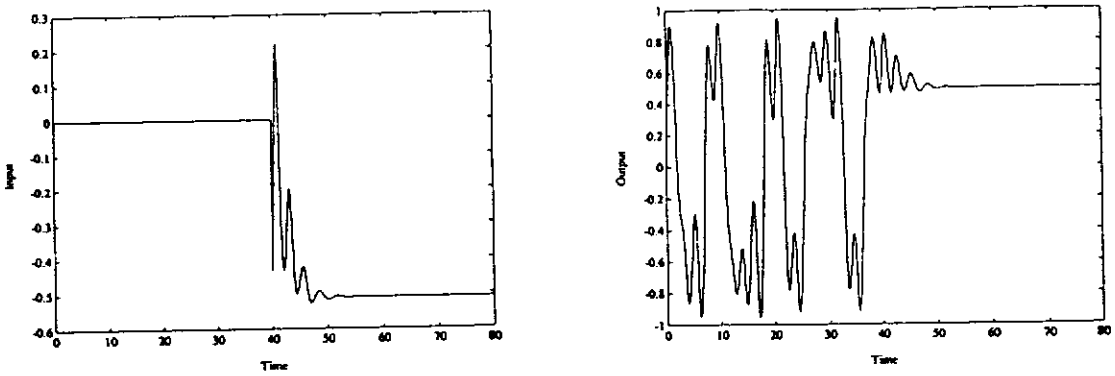

(a) (b)

Fig. 29. Tracking achieved by optimal state feedback (reference input $r = 0.5$): (a) Control signal $u(t)$; (b) Output $x(t)$. (*Figure from Hartley & Mossayebi [1993]*.)

4.3.4. *Occasional proportional feedback control*

As mentioned earlier (Sec. 2.2.3), the occasional proportional feedback (OPF) method also belongs to the category of engineering control approaches. The OPF method can be used to control and track periodic orbits as well as the non-oscillatory unstable state of Chua's circuit.

In Johnson *et al.* [1993], this method was applied to Chua's circuit. They chose to perturb the magnitude of the negative resistance since "it does not alter the natural frequency of the system in a first order approximation." The overall negative resistance is obtained by letting a fixed nonlinear resistance be in parallel with a voltage-variable resistance (VVR) which is provided by a field-effect transistor. The control of the system is achieved by modulating this VVR. Since the system is autonomous, an external synchronizing signal (with frequency f_{sync}) is used and is supplied by a separate signal generator. The circuit implementation is shown in Fig. 30. Similar to the diode resonator case, the voltage V_R is sampled and fed back to the window comparator where it is compared to the offset control voltage V_{set}. When the voltage peak falls within the comparator, the gate switches a signal proportional to $(V_{R,\text{peak}} - V_{\text{set}})$, which is then amplified to become the feedback control voltage signal V_{VVR}. In the experiment, the circuit oscillates chaotically until it visits the neighborhood of the fixed point (i.e., inside the window), then the proper feedback control signal ensures that on the next cycle, the circuit solution trajectory approaches the fixed point. To control the circuit so that the two basins of attractions of the double scroll are visited, two separate controllers are used

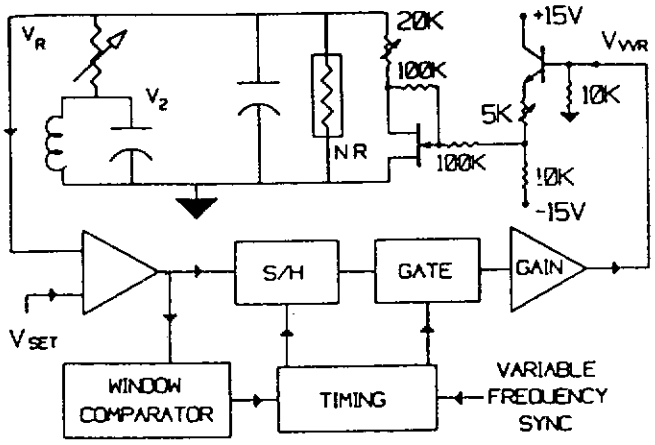

Fig. 30. Implementation of OPF control of Chua's circuit. (*Figure from Johnson, Tigner & Hunt [1993].*)

and a window comparator is set in each of the two basins. By summing up the outputs of the two controllers, corrections can be applied during visits to both basins during one stabilized orbit.

Johnson & Hunt [1993] described how to control the unstable fixed point of Chua's circuit by using the OPF technique together with the continuation method discussed in Carrol *et al.* [1993]. For this purpose, the negative resistance is set such that there is a dc voltage across the negative resistance. A stable fixed point will become unstable or even chaotic as one reduces the negative resistance. They set f_{sync} near the frequency of the period-1 limit cycle and adjusted approximately the set-point voltage V_{set} to the voltage of the steady-state solution. During the control process, V_{set} and f_{sync} are adjusted again to stabilize the equilibrium point with a minimum correction control signal, and the oscillations are reduced to a level comparable to the noise. As the negative resistance is decreased further, the dc voltage level increases, and so does V_{set} to ensure the minimum control energy. Repeated adjustment of the negative resistance and V_{set} will allow the fixed point to be tracked well into the chaotic regime.

4.3.5. *Distortion control*

Genesio and Tesi have recently proven the possibility of using the frequency harmonic balance (HB) technique for investigating complex behavior of nonlinear systems (prediction of chaos). They proposed some simple structural (non-numerical) conditions to recognize approximately the chaos onset, and employed nonlinear feedback to suppress certain chaotic phenomena [Genesio & Tesi, 1992, 1993].

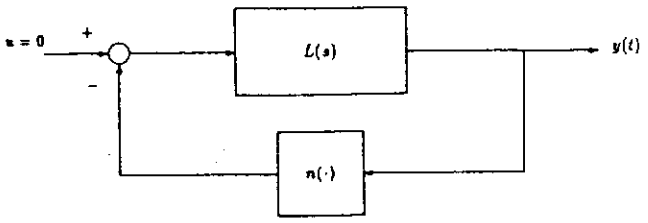

Fig. 31. A dynamical system in Lur'e form. (*Figure from Genesio & Tesi [1993].*)

Their research has led to a design procedure which can yield "qualitatively correct, though not exact, results in a quite simple way" [Genesio & Tesi, 1993].

As for many unforced systems, a feedback structure (Lur'e system) like the one shown in Fig. 31 can be derived from the state equations of Chua's circuit, where $L(s)$ denotes the transfer function of the linear part and $n(\cdot)$ represents a single valued nonlinear function of the system. Here, assuming $g(v_{C_1}) = -m_2 v_{C_1} + m_3 v_{C_1}^3$ and letting $y = v_{C_1}$, it follows that

$$L(s) = \frac{p(s^2 + s + q)}{s^3 + (1+p)s^2 + qs + pq}, \qquad n(y) = -\frac{m_2}{G}y + \frac{m_3}{G}y^3, \tag{57}$$

where p and q are system parameters. After the chaotic behavior of the system has been recognized by means of HB analysis [Genesio & Tesi, 1993], in order to control the chaos onset and to drive the system to the fundamental periodic solution $y_0(t) = A + B\sin(\hat{\omega}t)$ (with constants A, B, $\hat{\omega} > 0$), they considered using the structure shown in Fig. 32

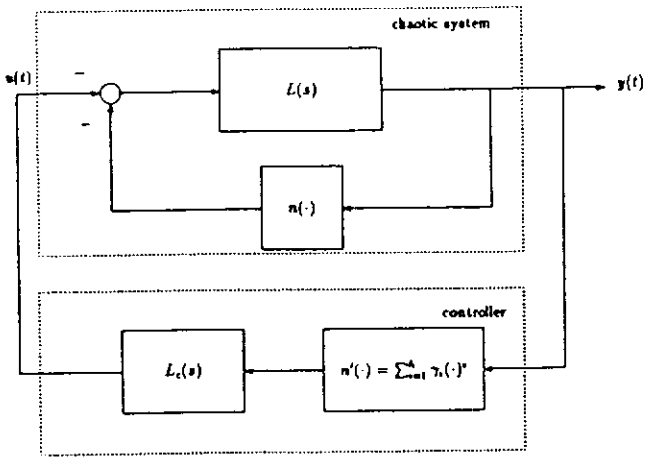

Fig. 32. Structure of the system for distortion control. (*Figure from Genesio & Tesi [1993].*)

where the nonlinear feedback controller contains a memoryless nonlinearity of the form

$$n'(y) = \sum_{1}^{h} \gamma_i y^i = \gamma_1 y + \gamma_2 y^2 + \gamma_3 y^3 ,$$
$$(h = 3 \text{ for Chua's circuit})$$

cascaded with a linear filter $L_c(s) = s/(s+\lambda)$. Then the design problem reduces to determining λ and γ_i, $i = 1, 2, 3$. Note that the term "distortion" refers to the relative amount of the neglected higher harmonics and is expressed by

$$\Delta = \frac{\|\tilde{y}_0(t) - y_0(t)\|_2}{\|y_0(t)\|_2} ,$$

where $\tilde{y}_0(t)$ is the steady state periodic output of the open-loop path of the system in response to $y_0(t)$. The so-called "distortion control" is to reduce the system distortion for the same predicted limit cycle, an approximate system solution derived by the describing function method. This controller design procedure preserves a number of systems characteristics (equilibrium points, stability properties, etc.) and the control energy used is quite low. Along this procedure, some of the structural conditions for recognizing nonlinear behavior are removed from the nonlinear feedback control system, and this results in the synthesization of the desired distortion control [Genesio & Tesi, 1993].

4.3.6. *Non-autonomous version of Chua's circuit and its control*

In addition to the study of the original Chua's circuit, there have been some research activities on the dynamics of the non-autonomous version of the circuit and its control [Murali & Lakshmanan, 1993]. Murali and Lakshmanan have been able to show that their non-autonomous version of Chua's circuit (an external periodic signal generator is connected in series to the inductor L) can also exhibit a rich variety of bifurcation routes to chaos. They have demonstrated the control of chaos in this forced Chua's circuit by adding a second periodic signal generator in series with the previous one such that the circuit becomes a quasiperiodically driven system. The addition of the second signal source and its proper adjustment seems quite effective in suppressing chaotic oscillations in the circuit [Murali & Lakshmanan, 1993].

4.4. *A stochastic control approach*

With their sensitive dependence on initial conditions and on system parameters, the trajectories of chaotic systems starting from any pair of arbitrarily close positions will diverge exponentially and become more and more uncorrelated with time. This characteristic is reminiscent of the "noise-corrupted" systems, where uncertainty or noisy measurement in the system cause progressive loss of information about the system states. This suggests that the uncertainty associated with the chaotic system state may be treated by a noise covariance matrix, and that the control of chaotic systems may be established in a manner akin to that of linear nondeterministic systems.

In 1989, Fowler [1989] constructed a system, as shown in Fig. 33, to bring out the "uncertainty" associated with a chaotic system of the form

$$\dot{\mathbf{x}} = F(\mathbf{x}, \mathbf{u}) , \tag{58}$$

where the uncertainty on the state of the system is represented by a covariance matrix

$$P = \text{cov}\{\mathbf{x}\} = E\{(\mathbf{x} - E\{\mathbf{x}\})(\mathbf{x} - E\{\mathbf{x}\})^\top\} . \tag{59}$$

The states $\mathbf{x}(t)$ of the chaotic system are sampled at fixed time intervals t_k, and these sample values $\mathbf{x}(t_k)$ are input to an estimation machanism, which yields the state estimate $\hat{\mathbf{x}}(t_k)$. The deterministic optimal control block will then use this estimate to develop an optimal control $u^*(t)$ $(t_k \le t < t_{k+1})$. The assumptions made here are that there is no plant noise [i.e., no noise within $\dot{\mathbf{x}} = F(\mathbf{x}, \mathbf{u})$] and the measurement noise or uncertainty associated with the system has Gaussian statistics. This uncertainty is further assumed to be related to the system dynamics through a second-order Fokker–Planck equation

$$\frac{\partial f(\mathbf{x}, t)}{\partial t} = \sum \frac{\partial}{\partial x_i} F_i(\mathbf{x}, u) f(\mathbf{x}, t) + \frac{1}{2} \sum_{i,j} Q_{ij} \frac{\partial^2 f(\mathbf{x}, t)}{\partial x_i \partial x_j} , \tag{60}$$

where $f(\mathbf{x}, t)$ is the joint probability density function of the state variables x_i, and the diffusion coefficients Q_{ij} are obtained from $P(t_k^+)$ at the beginning of a propagation cycle. The solution of the above equation is used to calculate the covariance matrix $P(t_k)$. Then, the covariance $P(t_k)$,

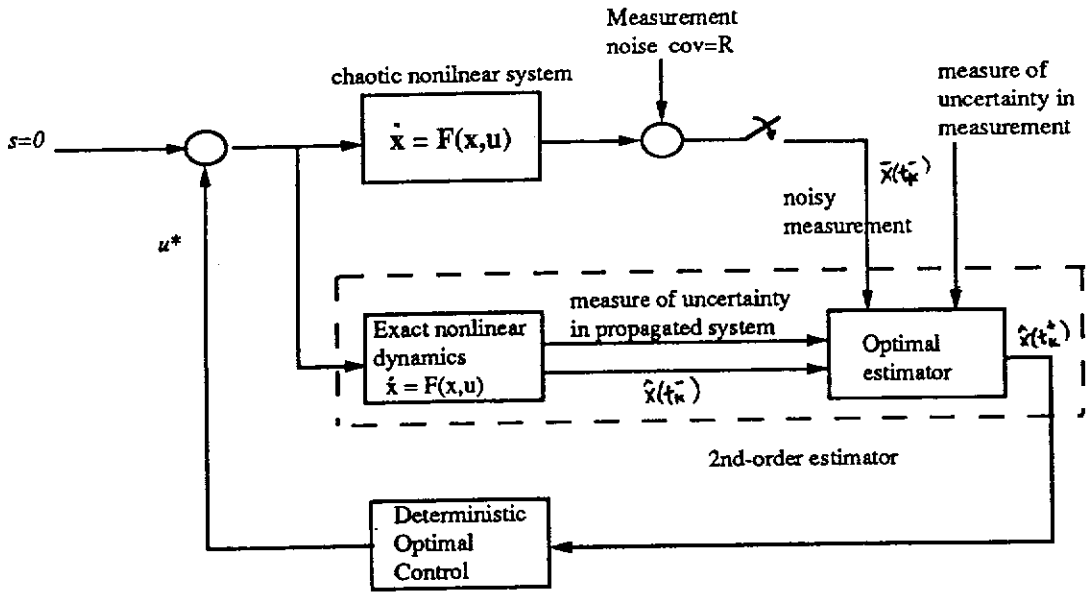

Fig. 33. Block diagram for the stochastic control system with a Kalman filter. (*This figure is based on a picture in Fowler [1989].*)

the measurement noise covariance R, the first moment $E\{\mathbf{x}\}(t_k^-)$, and the propagated mean $\hat{\mathbf{x}}(t_k^+)$ will be input to the second-order estimator based on a Kalman filter. The control technique was applied to the Hénon–Heiles system, which, when being controlled, takes the form

$$\begin{cases} \dot{x}_1 = x_3\,, \\ \dot{x}_2 = x_4\,, \\ \dot{x}_3 = -x_1 - 2x_1x_2 + u_1\,, \\ \dot{x}_4 = -x_1^2 - x_2 + x_2^2 + u_2\,. \end{cases} \tag{61}$$

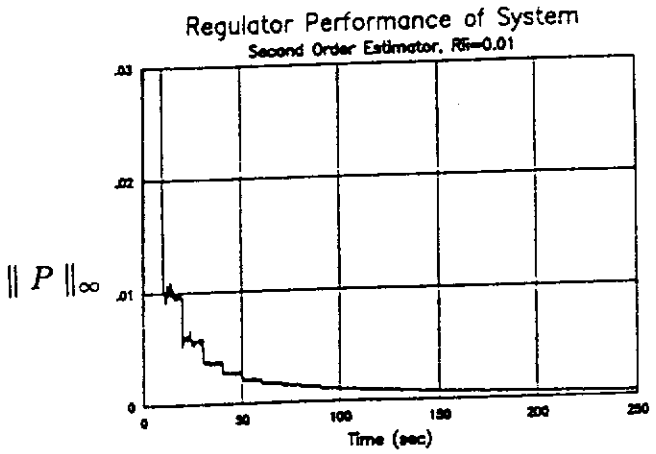

Fig. 34. System performance in terms of $\|P\|_\infty$. (*Figure from Fowler [1989], courtesy of IEEE; ©1989 IEEE.*)

With the goal to minimize the cost function $J = \int_{t_0}^{t_f}(x_1u_1^2 + x_2u_2^2)dt$ for some terminal time $t_f > t_0$, Fowler carried out some regulator and control problem-related experiments on the system of Fig. 33. He reported that the system is not completely controllable, and the uncontrolled system becomes unstable for values of total energy greater than 1/6, which may cause the failure of the control algorithm. Nevertheless, his simulation results show that employment of the Kalman filter does improve stability of the system and significantly reduce the uncertainty encountered in the system, as depicted in Fig. 34, where the uncertainty is quantified by the L_∞-norm of the covariance matrix P, $\|P\|_\infty$.

4.5. *A two-degree-of-freedom robust controller*

In 1991, Kameda, Aihara and Hori designed a two-degree-of-freedom (TDOF) robust controller for the purpose of reducing chaos of a control system [Kameda *et al.*, 1991]. The objective was actually two-fold: to reject chaotic disturbance and to control a chaotic plant.

The configuration of this TDOF robust controller is illustrated in Fig. 25(a), where r, d, and n are the reference input, disturbance, and

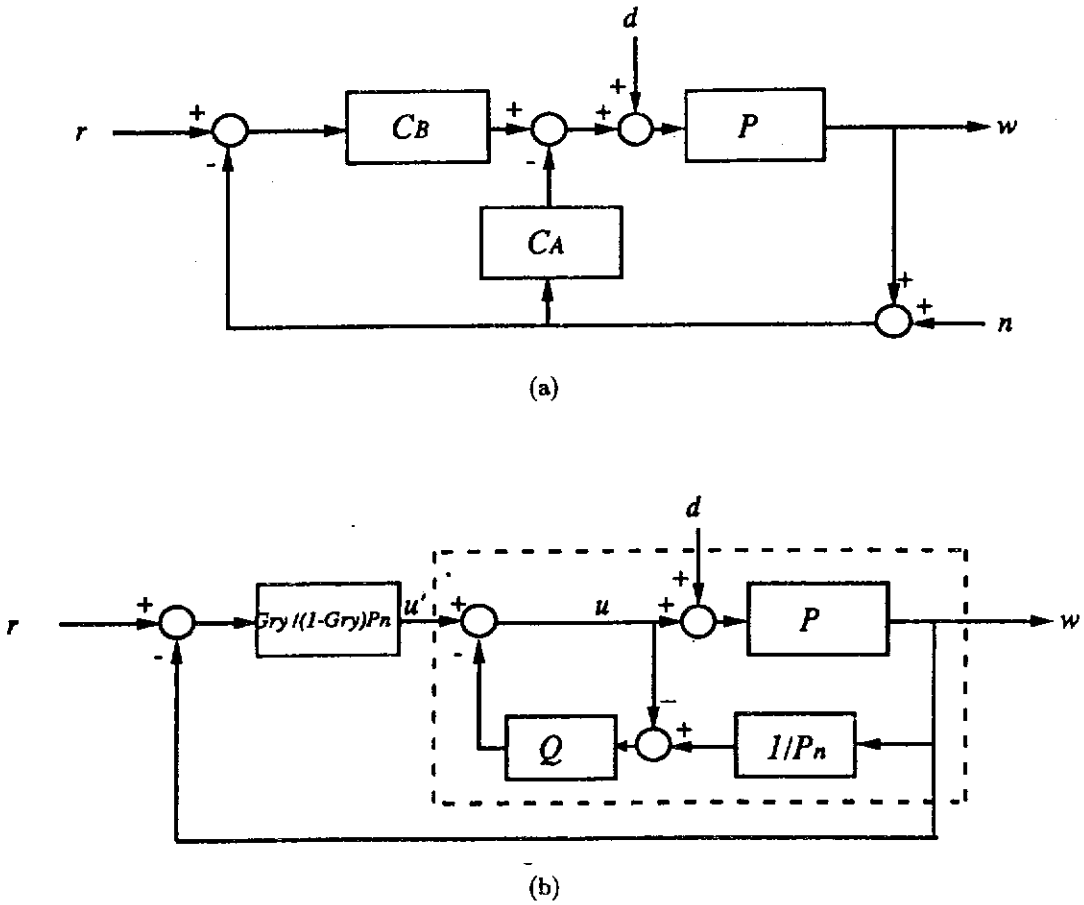

Fig. 35. Configuration of the TDOF robust controller. (*This figure is based on a picture in Kameda, Aihara & Hori [1991].*)

observation noise respectively, and

$$C_A(s) = \frac{Q(s)}{P_n(s)(1-Q(s))},$$

$$C_B(s) = \frac{G_{ry}(s)}{1-G_{ry}(s)} \cdot \frac{1}{P_n(s)(1-Q(s))},$$

in which $P_n(s)$ is the nominal model (system) of the plant P, $G_{ry}(s)$ is the reference model of the command input response, and $Q(s)$ is a strictly proper low-pass filter.

An equivalent block diagram of Fig. 35(a) is shown in Fig. 35(b), where the part inside the dashed boundary is to perform the nominalization of the plant P.

To study the suppression of chaotic noise, the disturbance d was produced by the well-known Lorenz equations

$$\begin{cases} \dot{x} = \sigma(-x+y), \\ \dot{y} = -xz + \gamma x - y, \\ \dot{z} = xy - bz, \end{cases} \tag{62}$$

with $\sigma = 10$, $\gamma = 28$ and $b = 8/3$. In their first simulation, x in the above equations was considered as the chaotic disturbance to the system. It was further assumed that

$$P = \frac{1}{1+Ts}, \; P_n = \frac{1}{1+T_n s}, \quad \text{and} \quad Q = \frac{1}{1+\tau s},$$

where T, T_n, and τ are time constants. The numerical results [Fig. 36(a) and 36(b)] indicate that the TDOF robust controller so designed can nominalize the plant and reject the chaotic disturbance.

In their second simulation, the effect of the same TDOF controller on the chaotic plant represented by the Lorenz equations has also been tested. The results of Fig. 37(a) and 37(b) are for the case where the output w is chosen to be the state x of the equations, and the control input u is added to $\dot{x} = \sigma(-x+y)$ to give $\dot{x} = \sigma(-x+y)+u$. Apparently, the chaotic plant is nominalized to some extent.

If $w = y$ and u is added to $\dot{y} = -xz + \gamma x - y$, results similar to Fig. 37(a) and 37(b) can be obtained. However, failure occurs if z is chosen as

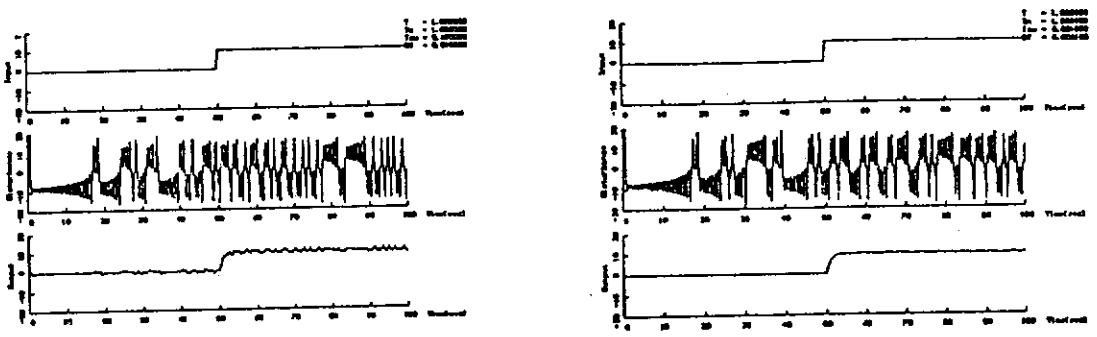

$\tau = 0.1$ (a) $\tau = 0.001$ (b)

Fig. 36. Response characteristics with chaotic disturbances ($T = 1$, $T_n = 1$). (*Figure from Kameda, Aihara & Hori [1991], courtesy of IEE of Japan.*)

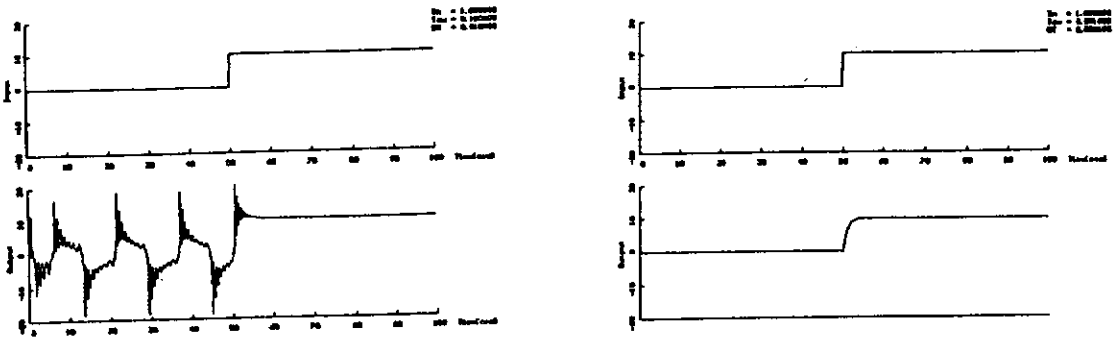

$\tau = 0.1$ (a) $\tau = 0.001$ (b)

Fig. 37. Waveforms of the input u' and the output $w = x$ under the influence of the TDOF robust controller (u is added to $\dot{x} = \sigma(-x + y)$). (*Figure from Kameda, Aihara & Hori [1991]), courtesy of IEE of Japan.*)

the output and u is added to $\dot{z} = xy - bz$ of the Lorenz equations, as reported in Kameda *et al.* [1991].

5. Other Approaches and Applications

Novel ideas and successful approaches to the control of chaos and other related topics, as well as their preliminary applications, are actually too many to describe in a survey paper of modest size, although most of them have just come out within the past few years. For this reason, we select, probably with personal biased preference, some of them to discuss in this last section of the paper.

5.1. *Controlling chaos in distributed systems*

A distributed artificial intelligence (DAI) system is usually composed of a very large number of interacting agents, and these many autonomous agents are expected to complete a variety of tasks cooperatively. To successfully complete one task, the individual agents have to make some important decisions, such as: Which problem-solving strategy to use? Or, with which other agents to interact? These decisions may also have to be changed in order to accommodate the new information that keeps arriving. Such information is usually about the state of the system and/or possibly about the decisions made by the other agents. However, complication arises if the information received by the

agent is conflicting, ambiguous, incomplete, or delayed. This "ill-conceived" information or misinformation will lead the agent to "make poor decisions when judged from a global perspective even though they appear locally reasonable," and chaos may then take place, therefore hampering the successful completion of the task.

There are a number of possible approaches in the control of DAI systems. Many of them are operational only for systems of a few agents, which deal with simple problems; they simply cannot cope with the complexity and/or nonlinearity in more realistic situations. Hogg & Huberman [1991] studied a simple yet representative DAI system, a computational ecosystem, and proposed an effective procedure for controlling the chaos in such a DAI system. The procedure uses a reward policy which increases the portion of agents that perform well, resulting in a robust control effect for the overall performance of the system.

5.1.1. *Chaos in DAI systems*

Assuming that the agents are of different types with different performance characteristics, and therefore, while making decisions they extrapolate information in different ways to estimate the state of the system. For purpose of exposition, let $f_{rs}(t)$ be the fraction of type-s agents using resource r at the time instant t. The total fraction of agents using resource r is defined to be $f_r^{\text{res}} = \sum_s f_{rs}$, and the total fraction of agents of type-s is $f_s^{\text{type}} = \sum_r f_{rs}$. Denote by $\rho_{rs}(t)$ the probability of that type-s agents will prefer resource r while making the choice. Let, moreover, $G_r(t)$ be the resource payoff for using resource r, which depends on the number of agents using the resource r. Note that only instantaneous resource payoffs are considered here. Now the dynamics of the computational ecosystem can be described by

$$\dot{f}_{rs} = \alpha(f_s^{\text{type}}\rho_{rs} - f_{rs})\,, \tag{63}$$

where α denotes the rate at which agents reevaluate their resource choice. Usually, $\rho_{rs}(t)$ is a function of $f_{rs}(t)$ through the payoffs $G_r(t)$. For the distributed system in which agents choose among two resources with cooperative payoffs, the dynamics of the fraction of agents using resource 1 is sufficient to describe the whole system:

$$\dot{f}_{1s} = \alpha(\rho_{1s} - f_{1s})\,. \tag{64}$$

In terms of the payoffs and uncertainty, the probability of that an agent will prefer resource 1 over 2 is

$$\rho_{1s} = \frac{1}{2}\left[1 + \operatorname{erf}\left(\frac{G_1(f_{1s}) - G_2(f_{1s})}{2\sigma}\right)\right], \tag{65}$$

where σ is the uncertainty, which is taken as the difference between the perceived payoffs and the actual ones. This representation indicates that an agent is more likely to prefer a resource when its payoff is relatively large in a cooperative environment.

Information delay makes obsolete agents' knowledge of the state of the system, and it can be modeled by supposing that the payoffs in Eq. (64) at time t are those at time $t - \tau$, where τ is the time-delay:

$$\rho_{1s}(t) = \frac{1}{2}\left[1 + \operatorname{erf}\left(\frac{G_1(f_{1s}(t-\tau)) - G_2(f_{1s}(t-\tau))}{2\sigma}\right)\right]. \tag{66}$$

Incomplete or conflicting information leads to deviation of the agents' perceived payoffs from the actual ones, which becomes larger when the information becomes less certain. In this kind of ill-informed environment, as mentioned earlier, the agents will tend to make poor decisions, which may result in chaos in the global dynamics of the system. Note that for simplicity, all agents are assumed to have the same effective time-delay, uncertainty, and resource preference. Figure 38 shows that with successively increasing τ, the fraction $f_{1s}(t)$ undergoes a series of behaviors of (a) converging to a stable equilibrium, (b) converging to a limit cycle, or (c) being chaotic. The payoffs used in this experiment are $G_{1s}(t) = 4 + 7f_{1s}(t) - 5.333f_{1s}^2(t)$ and $G_{2s}(t) = 4 + 3f_{1s}(t)$. Note that the initial value $f_{1s}(0) = 0$ implies that all agents start with using resource 2.

5.1.2. *Using reward policy to control chaos in DAI systems*

To overcome the chaotic behavior like the one shown in Fig. 38(c), Hogg & Huberman [1991] proposed to introduce to a computational ecosystem a reward mechanism that rewards agents according to their actual performance. Regardless of its implementation, the reward mechanism is supposed to increase the proportion of highly-performing agents and at the same time decrease the number of those who did not work well.

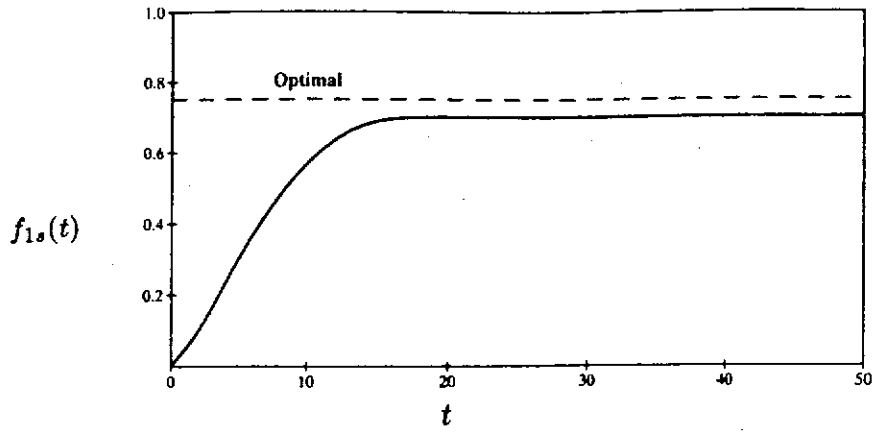

(a)

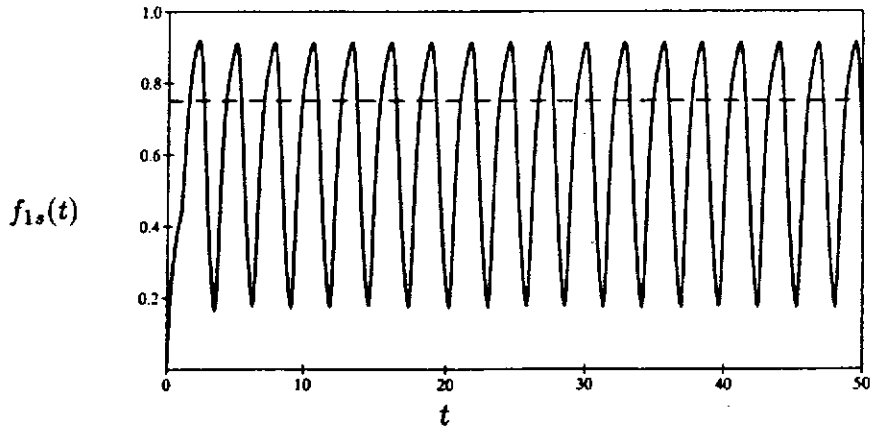

(b)

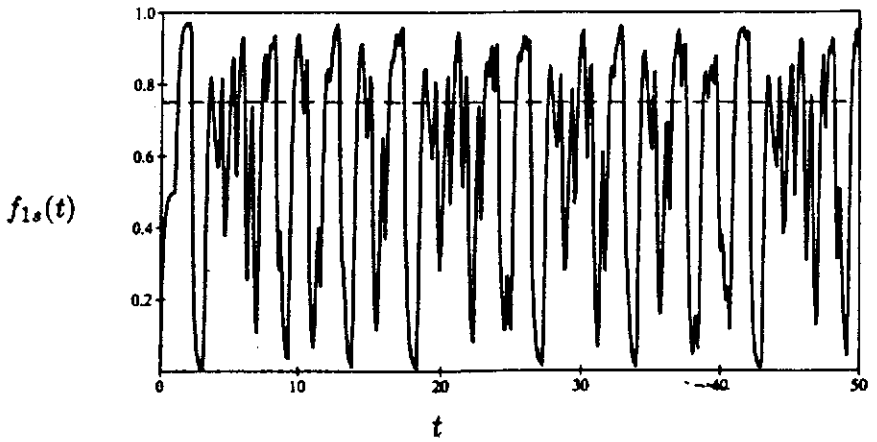

(c)

Fig. 38. Behaviors of $f_{1s}(t)$ for successively longer delays τ, with $\sigma = 0.25$. (*Figure from Hogg & Huberman [1991], courtesy of IEEE;* ©*1991 IEEE.*)

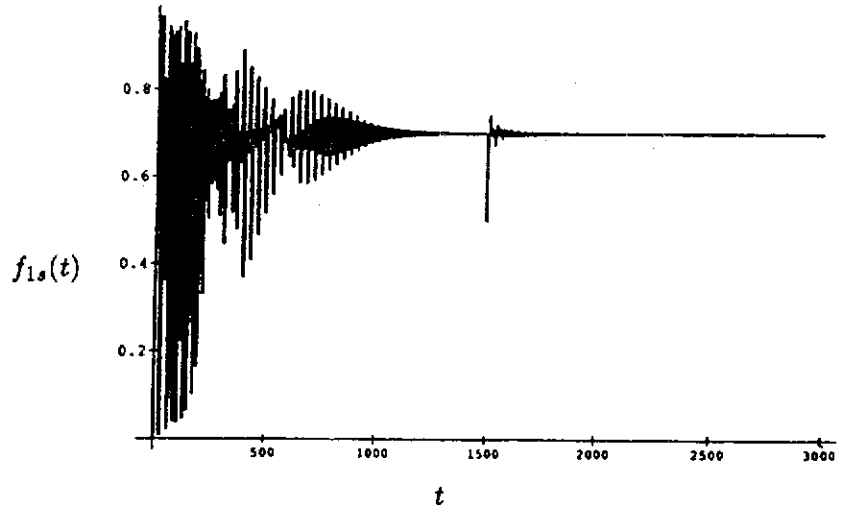

Fig. 39. Behavior of $f_{1s}(t)$ with adjustment from actual payoff. $\sigma = 0.25$, $\tau = 10$. (*Figure from Hogg & Huberman [1991], courtesy of IEEE*; ©*1991 IEEE.*)

Note that the actual payoff received by type-s agents is $G_{\text{actual},s} = \sum_r f_{rs} G_r$, whereas the total payoff for all agents is $G_{\text{total}} = \sum_r f_r^{\text{res}} G_r$, both normalized to the total number of agents in the system. Then the relative payoff or the probability of that new agents will be of type s is

$$\eta_s = \frac{G_{\text{actual},s}}{G_{\text{total}}} = \frac{\sum_r f_{rs} G_r}{\sum_r f_r^{\text{res}} G_r},$$

which is proportional to the actual payoff. Taking into account the reward policy, system dynamics become

$$\dot{f}_{rs} = \alpha(f_s^{\text{type}} \rho_{rs} - f_{rs}) + \gamma(f_r^{\text{res}} \eta_s - f_{rs}), \quad (67)$$

in which the second item corresponds to the reward mechanism, and γ is the rate at which the actual performance is rewarded. The physical meaning of γ depends on what kind of reward mechanism is used.

Now, it is easy to see that

$$\dot{f}_r^{\text{res}} = \alpha \left(\sum_s f_s^{\text{type}} \rho_{rs} - f_r^{\text{res}} \right) \quad (68)$$

describes the dynamics of the overall resource use, and

$$\dot{f}_s^{\text{type}} = \gamma(\eta_s - f_s^{\text{type}}) \quad (69)$$

represents the distribution of agent types, where the number of those agent types who receive payoff greater than the average (i.e., agents with $\eta_s > f_s^{\text{type}}$) will increase and that of poorly performing agents will decrease.

Sufficient diversity of agents is needed to make the system stable. Hogg and Huberman took the diversity to correspond to the different extra delays used by the agents to estimate the current state of the system. Namely, different types (of agents) correspond to different assumed periods: type-s agents will use effective delays of $\tau + s$ when their decisions are evaluated. They then ran the same experiment as that of Fig. 38(c) but, this time, rewarded the actual performance or actual payoff of the agents. When the extra delay is within the range from 0 to 40 (time units), the dynamics generated by Eq. (66) is shown in Fig. 39: $f_{1s}(t)$ first goes through a chaotic transient, then gradually settles down to the equilibrium point which is unreachable in the absence of a reward mechanism. It can be observed that the introduction of perturbation does not affect the eventual stability of the system.

The essence of Hogg and Huberman's approach is that rewarding well-performing agents in a large collection of agents engaging in resource choices generates a high degree of diversity of agents, and this diversity will eventually stabilize the system by eliminating chaotic behavior through a sequence of dynamical bifurcations. Although many open problems remain, the concept of rewards does shed some significant insight into the understanding and design of complex distributed artificial intelligence systems.

5.2. *Intelligent control of chaos*

Intelligent machines are envisioned to be adaptive, robust, and fault-tolerant. They are considered to

be good candidates for satisfactory operations of nonlinear systems embedded with a great deal of uncertainties.

For industrial processes and power plants, where the processes to be controlled are usually distributed and nonlinear due to their very nature with extensive process and disturbance uncertainties, one would desire a real-time intelligent control in place.

Artificial intelligent systems, expert systems, fuzzy systems, and neural network systems are among the most important intelligent machine technologies that have emerged. For an intelligent control configuration, expert systems may be used as adaptive elements, fuzzy systems as decision-making components, whereas neural networks may be implemented as compensation elements. Neural networks are attractive for the control purpose mainly due to their easy implementation, relatively simple structure, robustness, and especially their ability to accommodate defective and/or changing components in the overall system. Because neural networks are taught by examples, they usually have fast adaptation rate, allow the processes to be remodeled quickly, and can deal effectively with interacting parameters.

Frison [1992] studied the possibility of employing neural networks to control the Duffing system $\ddot{x} + p_1\dot{x} + p_2x + x^3 = q \sin \omega t$. A feedforward neural network is used to dampen the chaoticity in this oscillator. The configuration of his simulation is shown in Fig. 40.

There are various ways of constructing the desired neural network. The number of the hidden layer and the sizes of the input, output, and each hidden layer all determine the performance of the designed network. The input to the network is a concatenated recent time history of the acceleration term $\ddot{x}$ in the chaotic Duffing equation. Noise is injected into the system as this will make the system more realistic.

The difference between the network's prediction of the acceleration and the acceleration calculated through numerical integration is taken as the system error. This error is passed back to the network to be used for the backward propagation learning (training). For the network controller to continuously control the oscillator, the network is trained after each sampling period.

In this simulation model, neural network and scaling mechanism constitute the control device in the system. An automatic gain control scheme scales the oscillator acceleration to the values acceptable to the network. Since the range of the network output is fixed, this output also needs to be scaled to the largest acceleration term that may be encountered. This scaled output value is then being added to the Duffing oscillator, providing a term that counters the displacement x.

The performance of this neural-network controlled system is measured by the average decibels of suppression (of the error) observed after learning enters the asymptotic region which is typical in backward propagation.

Frison identified three distinct stages of learning experienced by the control device. When the system first starts, the network-response reflects how the initialization of the network has been done. As the network begins to learn the overall system dynamics, its response begins to reflect this dynamics. In fact, at this second stage, the network is learning to suppress higher-frequency oscillation components. Finally, the network is able to suppress the last non-fundamental frequency component, and it shifts to direct opposition of the

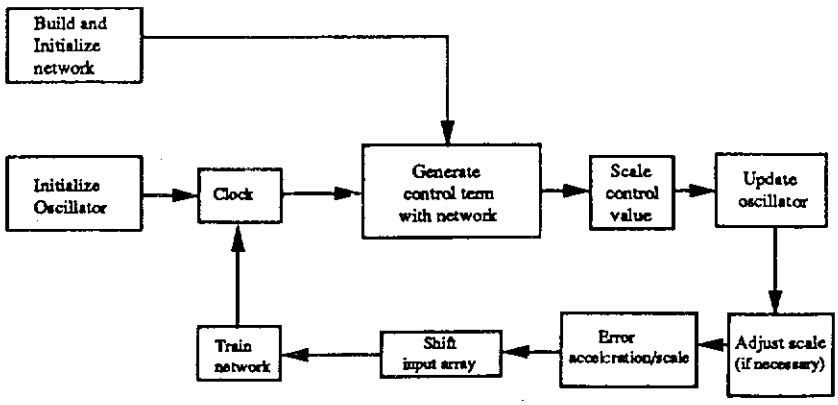

Fig. 40. Simulation of using neural network to control Duffing system. (*This figure is based on a picture in Frison [1992].*)

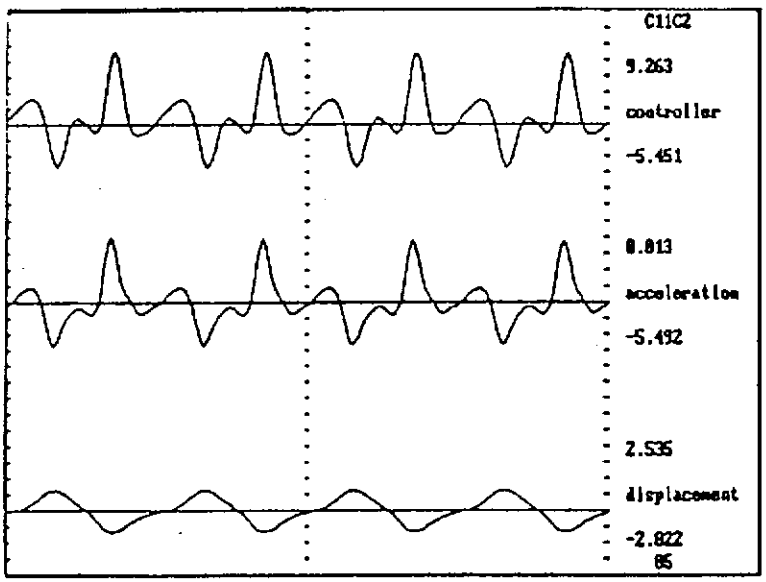

Fig. 41. Signal trace as the network learns to control the overall system. (*Figure from Frison [1992].*)

underlying forcing function $q \sin \omega t$. Now the controller's output replicates the forcing term in the Duffing equation, and the acceleration $\ddot{x}$ and displacement x are also reduced to sine waves as shown in Fig. 41.

It seems worth mentioning that there remain some difficulties associated with using or designing a neural network to control chaos. For example, there is no general way of deciding what kind of network topology to use for performing a particular control task, and the convergence of many of the popular learning algorithms used by neural networks is not yet guaranteed. Also, Frison's simulation model seems to be far from being failure-proof, and many other problems still remain. However, using neural networks or other types of intelligent machines to control chaos nevertheless have great potential, and hence deserves further exploitation.

5.3. *Signal encoding in a chaotic environment*

In early 1980s, Rapp, Mees and Sparrow argued that frequency-regulated control systems may be immune to chaos in the same way as they are immune to noise; this proposition came out as a result of their research on biological systems [Rapp *et al.*, 1981].

They first noted that many engineering systems use A/D and D/A control devices to encode information in the frequency. The practical benefit of this encoding process is the increased resistance of the system to noise corruption and the enhanced precision of the control. Rapp *et al.* referred to this process as "oscillatory regulation (or control)." They further contended that many of the biological oscillations in physiological systems (e.g., cardiac pacemaker, oscillations in secretary cells, and neural oscillations) represent some kind of biochemical implementation of the A/D or D/A strategy used for engineering systems, and that is how the stable and precise regulation of the biological system is achieved.

To be more concrete, Rapp *et al.* proposed the following protocol (shown in Fig. 42) for the general biological oscillation, where the process has three stages:

(i) the external analog demand signal is received by the cell (e.g., the concentration of hormone stimulating secretive cells);
(ii) this input signal activates a mechanism which generates a cellular oscillation, and the magnitude of this signal determines the frequency of this oscillation (e.g., the membrane potential oscillation); and
(iii) this oscillation then drives a frequency-dependent response mechanism, which in turn produces the resulting output response, a cellular response (e.g., the neurotransmitter release rates in neurons).

It was argued by Rapp *et al.*, [1981] that this protocol provides an efficient and noise-resistant mechanism. The conjectures made therein, which

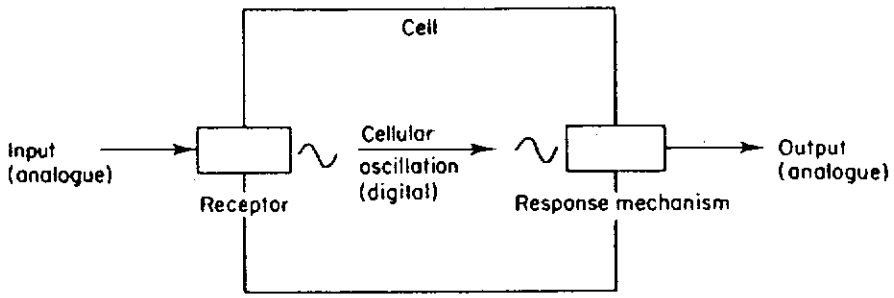

Fig. 42. A biological process. (*Figure from Rapp, Mees & Sparrow [1981], courtesy of Academic Press.*)

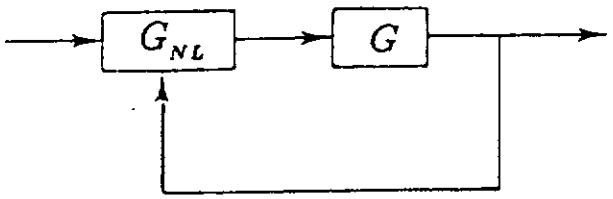

Fig. 43. Block diagram of a feedback system modeling the biochemical process of calcium-cyclic nucleotide interactions. (*This figure is based on a picture in Rapp, Mees & Sparrow [1981].*)

are of interest to this survey, are the following: the conversion of the input signal to a cellular frequency signal is stable against the corruption by the input noise and, more significantly, even if the mechanism that generates the above signal conversion is involved in certain internal chaotic motion, the cellular frequency is "likely to be fairly stable and to be an accurate reflection of the magnitude of the input signal." They stated that it can be shown that this is typical for many metabolic control systems.

In particular, Rapp *et al.* used a simplified model (Fig. 43) to describe the complex biochemical process of an oscillator circuit in *Calliphora* salivary gland. In this model, the nonlinear component $G_{NL}(\cdot)$ receives the hormone signal and the calcium feedback signal, and is determined by the kinetic properties of the adenylate cyclase. The linear part, $G(\cdot)$, represents the intermediate reactions between the cyclic AMP synthesis by the adenylate cyclase and the control of the cytosol calcium. An analysis of this model using describing function method led to the following two statements: (1) The oscillation frequency is determined by $G(\cdot)$ and not by $G_{NL}(\cdot)$; (2) If subject to noise input, the model (Fig. 43) is approximately equivalent to a corresponding noise-free system which has a different nonlinear component but the same linear part. Based on the above arguments, they declared that frequency encoding in physiological oscillator is insensitive to noise and that the information of the demand signal is likely to be preserved even if this oscillation is of chaotic type.

As an example, consider $G(s) = 1/[1 + (s/n)]^n$ and $G_{NL}(x) = xre^{-x}$. Also assume that $n = 50$ and $r = 22$. The corresponding state-space description is

$$\begin{cases} \dot{x}_1 = [G_{NL}(x_n) - x_1]n\,, \\ \dot{x}_i = (x_{i-1} - x_i)n\,, \qquad (i = 2, 3, \ldots, 50(= n)) \end{cases} \tag{70}$$

and the chaotic behavior of $x_1(t)$ is shown in Fig. 44. It can be observed that with two different initial conditions, while the two amplitudes become more and more unrelated, their frequencies are almost the same. Similar properties have also been observed in other chaotic systems. Rapp *et al.* suggested that "the principal feature of chaotic motion is frequently a pronounced irregularity in amplitude" and that the period of motion in many cases "does not significantly vary from some average value" even though it does display seemingly random variations. In other words, the underlying frequency is comparatively stable. Thus, they concluded that "frequency encoded control networks need not suffer a disastrous loss of control if the system enters a chaotic regime while amplitude dependent control systems would almost certainly do so" [Rapp *et al.*, 1981].

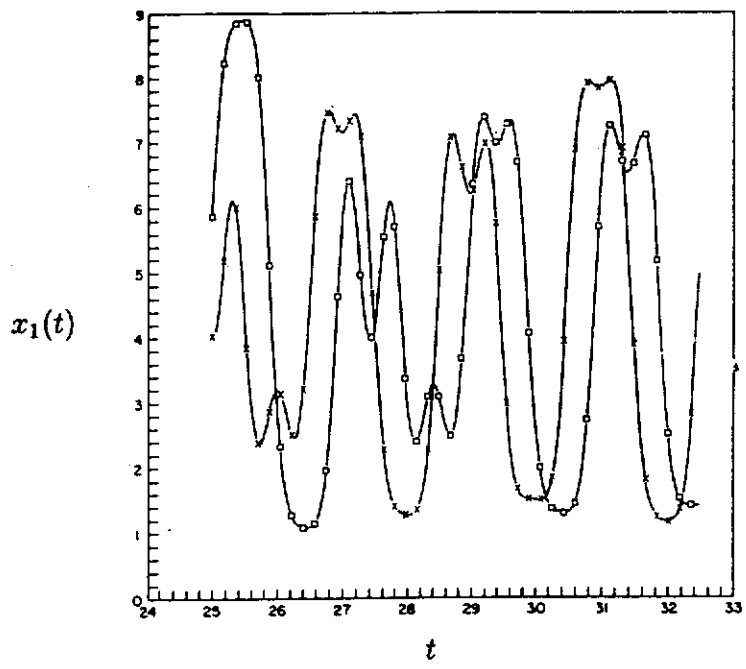

Fig. 44. Chaotic behavior of the state $x_1(t)$. (*Figure from Rapp, Mees & Sparrow [1981], courtesy of Academic Press.*)

The implication of their arguments is: if one knows that chaotic behavior (whether it is desired or not) is bound to occur in the system, he may purposely encode the control signal in frequency (rather than in amplitude) — in much the same way as that biological oscillations encode demand signals in cellular frequencies — to avoid possible destruction to the signal by the chaos.

5.4. *Using chaotic signals to synchronize dynamical systems*

As contrasted with the usual approaches where constant or periodic forces are used to control dynamical systems, the concept of using aperiodic or even chaotic signals as driving force is quite novel. The research activity motivated by this new concept is a perfect example that researchers have begun to look for applications of the intrinsic properties of chaotic systems. Plapp & Hübler [1990] showed that small-amplitude aperiodic signal can transform the rf-biased Josephson junction from a stationary state to the rotating state and result in nonchaotic dynamics. Pecora and Carroll, on the other hand, also pointed out that there are other occasions "when a chaotic signal would be preferable to a periodic signal as a drive or timing signal," and they developed a relatively more complete theory on synchronizing dynamical systems with chaotic signals [Pecora & Carroll, 1990, 1991; Carrol & Pecora, 1991].

5.4.1. *Concepts of drive and response subsystems*

Pecora and Carroll suggested to first decouple an n-dimensional autonomous system, $\dot{\mathbf{x}} = F(\mathbf{x})$ into two subsystems where the k-dimensional response subsystem $\dot{\mathbf{x}}_R = F_R(\mathbf{x}_D, \mathbf{x}_R)$ $(k < n)$ depends on variables of the $(n-k)$-dimensional drive subsystem $\dot{\mathbf{x}}_D = F_D(\mathbf{x}_D)$. One can move one step further to classify the variables $\mathbf{x}_D$ of the drive subsystem into a subset of m driving variables that actually "drive" the response subsystem and a subset of $n-k-m$ variables that do not. This results in an m-dimensional $\dot{\mathbf{x}}_d = F_d(\mathbf{x}_d, \mathbf{x}_{nd})$ and an $(n-k-m)$-dimensional $\dot{\mathbf{x}}_{nd} = F_{nd}(\mathbf{x}_d, \mathbf{x}_{nd})$. Correspondingly, the responding variables $\mathbf{x}_r$ form the response subsystem $\dot{\mathbf{x}}_r = F_r(\mathbf{x}_d, \mathbf{x}_r)$. The above decomposition process is best illustrated as follows:

$$\dot{\mathbf{x}} = F(\mathbf{x}) \Longrightarrow \begin{cases} \dot{\mathbf{x}}_D = F_D(\mathbf{x}_D) \\ \dot{\mathbf{x}}_R = F_R(\mathbf{x}_D, \mathbf{x}_R) \end{cases} \Longrightarrow \begin{cases} \begin{cases} \dot{\mathbf{x}}_d = F_d(\mathbf{x}_d, \mathbf{x}_{nd}), \\ \dot{\mathbf{x}}_{nd} = F_{nd}(\mathbf{x}_d, \mathbf{x}_{nd}), \end{cases} \\ \dot{\mathbf{x}}_r = F_r(\mathbf{x}_d, \mathbf{x}_r), \end{cases} \tag{71}$$